Ocean Engineering 265 (2022) 112624

Contents lists available at ScienceDirect

Ocean Engineering

journal homepage: www.elsevier.com/locate/oceaneng

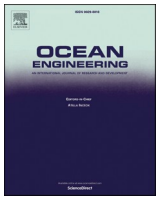

Flow characteristics on the leeside of a geotextile mattress with floating plate

Yehui Zhu [a], Liquan Xie [b,*], Tsung-chow Su [c]

[a] School of Environment and Architecture, University of Shanghai for Science and Technology, 516 Jungong Road, Shanghai, 200093, China
[b] College of Civil Engineering, Tongji University, 1239 Siping Road, Shanghai, 200092, China
[c] Department of Ocean and Mechanical Engineering, Florida Atlantic University, Boca Raton, FL, 33431, United States

ARTICLE INFO

Keywords:
Geotextile mattress with floating plate
Flow pattern
Bottom vortex
Blockage effect
Steady current

ABSTRACT

The Geotextile Mattress with Floating Plate (GMFP) is a novel scour prevention structure. This paper provides an insight into the effects on the flow pattern near the GMFP to better understand the GMFP working mechanism. The GMFP design parameters were emphasized, including the sloping angle, the height of the floating plate, and the opening ratio. In most cases, the bottom vortex is located immediately downstream to the GMFP. The near bottom velocity downstream to the bottom vortex is remarkably lower than the undisturbed value. The location variation of the bottom vortex reattachment point with the GMFP design parameters was studied. Within the range of hydrodynamic parameters tested, the reattachment point moves upstream when the opening ratio increases over 0.231, which agrees with previous studies. With the increase of the obstruction height of the floating plate, the reattachment point tends to move downstream when the relative obstruction height is below 0.2, and then retreats to the upstream side, which may be attributed to the variation in the water surface profile and the enhanced flow through the sand-pass gap due to the intensified blockage effect. An equation was proposed to predict the location of the reattachment based on the GMFP obstruction height.

1. Introduction

In coastal areas, local scour is always a threat to underwater structures like bridge piers, pipelines, and offshore wind turbines. Due to the effects of marine hydrodynamic forces, local scour can develop near marine structures and destabilize their foundations, leading to the failure of these structures. Such failures can bring catastrophe to both the economy and the ecological environment. For instance, when local scour develops at bridge piers (Fig. 1), the foundations of the piers can expose, which can endanger the stability of the bridges. The bridges suffering pier scour may eventually fail and thus cause local traffic paralysis and even casualties. As a result, scour protection measures have become the focus of many studies in the past decades.

At present, the countermeasures against scour can mainly be divided into two categories based on their working mechanism: covering the area vulnerable to scour and adjusting the local flow pattern. The former mainly includes ripraps (Biswas and Barbhuiya, 2018; Jafarnejad et al., 2019; Rashno et al., 2020), mattresses (Galan et al., 2015; Ma et al., 2021), and revetments (Kiss et al., 2019; Khajenoori et al., 2021), while the latter includes traditional groins (Cai et al., 2018; Zhang and Stive, 2019; Wu et al., 2022), submerged breakwaters (Li et al., 2021; Xue et al., 2022; Zhao et al., 2021), and floating flow-deflection devices.

The floating flow-deflection device is a series of flexible scour protection structures proposed in recent years, which includes the suspended flexible curtain (Li and Yu, 2009), the rigid suspended curtain (Wang et al., 2015), the geotextile mattress with sloping curtain (Xie et al., 2013), and the geotextile mattress with floating plate (Xie et al., 2019a; Zhu et al., 2020). These structures are capable of protecting the riverbed and seabed from scour by adjusting the local flow pattern, and some of them can also enhance sediment deposition on their leeside by providing a passage for the approaching bed load. The floating flow-deflection device is applicable to various conditions, including protecting underwater structures from local scour, and preventing bank collapses due to the erosion on riverbanks.

Many researchers have focused on the working mechanism and the protective effects of the floating flow deflection devices. Li and Yu (2009) revealed the flow pattern on the leeside of a suspended flexible curtain in steady currents with visualization tests. Two equations were proposed for the scale of the primary recirculation zone based on the blockage height and the sloping angle of the curtain. Later, Wang et al.

* Corresponding author. 1239 Siping Road, Shanghai, 200092, China.
E-mail address: xie_liquan@tongji.edu.cn (L. Xie).

https://doi.org/10.1016/j.oceaneng.2022.112624
Received 24 July 2022; Received in revised form 7 September 2022; Accepted 15 September 2022
Available online 29 September 2022

(2015) replaced the flexible curtain with a floating rigid curtain, and systematically investigated hydrodynamic characteristics of the floating rigid curtain. A series of empirical equations were established to predict the sloping angle of the curtain, the size of the recirculation zone, and the forces on the curtain in various flow conditions.

Xie et al. (2013) proposed the geotextile mattress with sloping curtain, and investigated the sediment deposition on the leeside of the structure in a steady current with a series of live bed flume experiments. The effect of the opening ratio of the curtain on the variation in the bed surface profile was discussed in detail. Later, the geotextile mattress with sloping curtain was introduced to the protection of the local scour under a submarine pipeline in steady currents (Xie et al., 2019b). The results indicated that the optimum protection effects are reached when the distance between the pipeline and the structure is about 6 times the obstruction height of the structure. Xie et al. (2015) studied the variation of the bed pressure distribution adjacent to the geotextile mattress with sloping curtain in regular waves.

The geotextile mattress with floating plate (GMFP) was recently proposed by Xie et al. (2019a) to improve the flexibility of floating flow-deflection device in both deployment and maintenance. The GMFP (Fig. 2) consists of a geotextile mattress and a floating plate. The geotextile mattress is the foundation of the device. The mattress is composed of a string of geotextile tubes filled with sand or concrete. The floating plate serves as a flow deflector. The plate is a rigid plate made of light materials, like polymer foam. A series of strings links the geotextile mattress with the bottom edge of the floating plate, forming a gap between the mattress and the floating plate. This gap provides a passage for the bed load and the near bottom flow, and is termed a sand-pass gap. Due to the buoyancy of the floating plate, the plate rises straight up in still water, and inclines to the downstream side in unidirectional currents. Belts are attached to the plate and the mattress to improve the integral stability of the structure.

The basic working mechanism of the GMFP is described as follows (Xie et al., 2019a). As is shown in Fig. 3, the floating plate of the GMFP inclines to the downstream side in a steady current. The floating plate divides the approaching flow into two parts. The upper branch climbs over the floating plate, and the lower branch passes through the sand-pass gap. The interaction of the two branches on the leeside of the GMFP creates two vortex systems: the top vortex zone and the bottom vortex. The top vortex zone is located near the upper edge of the floating plate and has limited effects on the bed. The bottom vortex is the main vortex on the leeside of the GMFP and covers a large area near the bed on the leeside of the structure. A safe area is formed from the bottom vortex and the low velocity zone, where the near bottom velocity is lower than that in the unprotected scenario. When the underwater structures are located within the safe area of a GMFP, the flow velocity and the sediment transportation capacity near the structure are reduced, and the structures can be protected from local scour. In addition, the bed load sediment in the bottom flow passing through the sand-pass gap can deposit in the safe area, and the scour potential is further reduced. More details of the GMFP working mechanism are reported by Xie et al. (2019a) and Zhu et al. (2020).

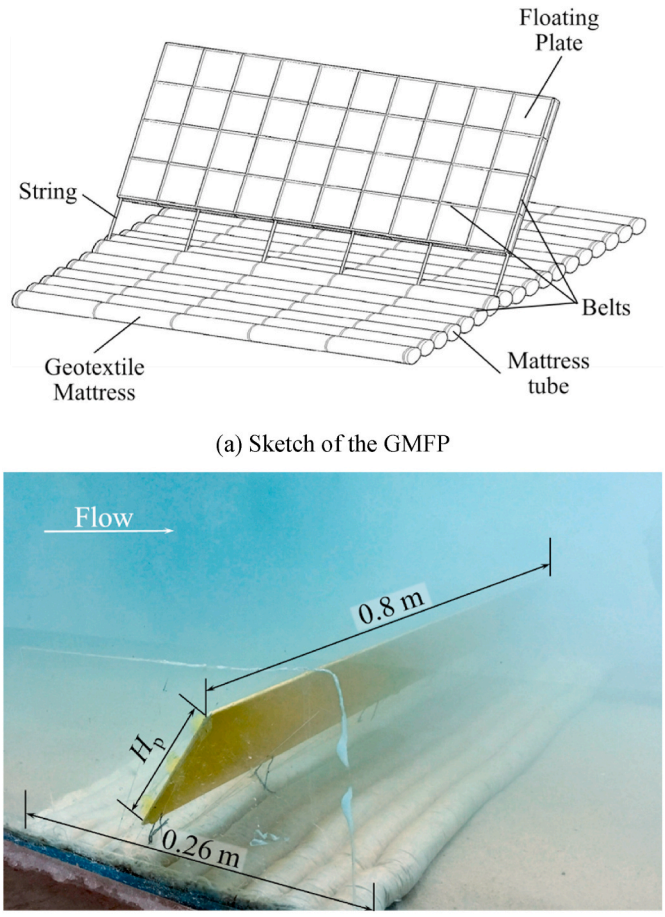

Fig. 2. (Color) Geotextile Mattress with Floating plate (GMFP) (Zhu et al., 2020). (For interpretation of the references to colour in this figure legend, the reader is referred to the Web version of this article.)

Some studies have been completed on the properties of the GMFP. Xie et al. (2019a) reported a bed pressure difference across the GMFP in a steady current. The bed pressure difference increases with the rise of the plate height and the sloping angle. The seepage stability of the GMFP was discussed in detail based on the flume experiment results. Zhu et al. (2020) validated the protection effects of the GMFP on the scour beneath a pipeline with flume experiments. The results indicate that the seepage

Fig. 1. (Color) Bridge pier before and after local scour (Lee et al., 2021). (For interpretation of the references to colour in this figure legend, the reader is referred to the Web version of this article.)

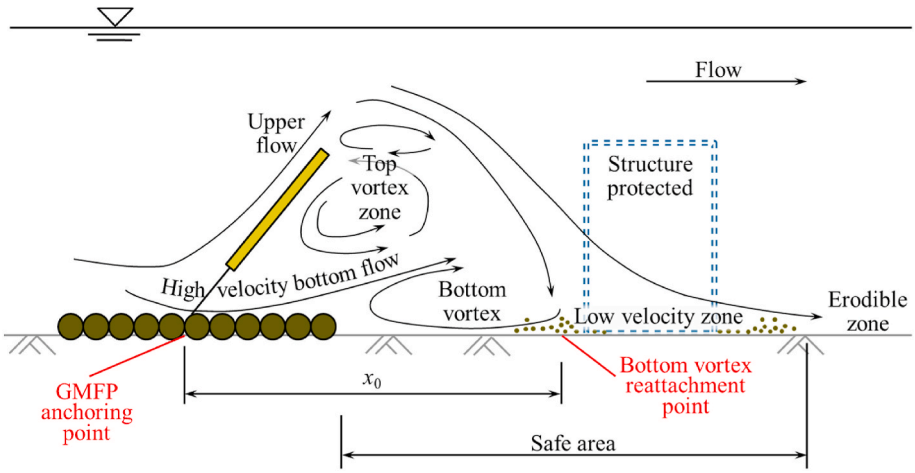

Fig. 3. (Color) Basic working mechanism of the GMFP. (For interpretation of the references to colour in this figure legend, the reader is referred to the Web version of this article.)

hydraulic gradient under the pipeline descends with the increase of the plate obstruction height.

Despite the knowledge amassed on the GMFP, many properties of the GMFP are still unclear. The flow pattern on the leeside of the GMFP is unknown, which has become a bottleneck of further investigations on the protection mechanism of the GMFP. Wang et al. (2015) reported the flow pattern on the leeside of a floating rigid curtain, which is a floating flow-deflection device similar to the GMFP. However, the flow patterns on the leeside of the GMFP and the floating rigid curtain are actually different due to the structural distinctions between the two devices. The GMFP is equipped with a geotextile mattress on the bottom, while the floating rigid curtain does not include such a part. The mattress covers the bed directly under the floating plate and increases the friction on the bed, slowing down the bottom flow through the sand-pass opening, and thus helping to prevent the local scour near the GMFP (Xie et al., 2013). The difference in the bottom flow can bring variation between the flow pattern on the leeside of the GMFP and that of the floating rigid curtain. Thus, the previous achievements cannot necessarily be applied directly to the GMFP, and it is essential to investigate the flow field characteristics on the leeside of a GMFP.

In addition, the sloping angle of the plate can significantly affect the flow pattern on the leeside of a GMFP. The effect of the sloping angle on the flow pattern has not been systematically reported. Many previous studies regarded the sloping angle as a function of the plate height and the hydrodynamic parameters. However, in practical engineering projects, the sloping angle can be adjusted intentionally by varying the density and the thickness of the floating plate when the designed flow velocity and the plate height of a GMFP are selected. Thus, the sloping angle is also regarded as an independent variable in the present study to better understand the properties of the GMFP.

In this study, a series of flume experiments were designed to study the flow field downstream to a GMFP by measuring the near bottom velocity. The aim of this qualitative study was to reveal the effects of the GMFP design parameters on the flow pattern. The effects of three GMFP design parameters were analyzed, namely the height of the floating plate, the sloping angle of the plate, and the opening ratio. The effects of these parameters on the characteristics of the flow field were discussed. The results of this study provide some elementary knowledge for future analysis on the working mechanism of the GMFP and its protection performance. The achievements of these investigations help to push forward practical applications of the GMFP, which will benefit the safety and stability of the submarine structures.

2. Methodology

2.1. Experiment method

The experiments were performed in a hydraulic flume at the Laboratory of Hydraulic and Harbor Engineering, Tongji University (Fig. 4). The flume is 50 m long, 0.8 m wide and 1.2 m deep, and is equipped with an automatic flow-generating system, which has a pump capable of generating a 1.0 m/s steady current at 0.4 m water depth. Two metal fences are installed at the entrance and exit of the flume to ensure a steady flow in the flume. The side walls of the flume are made of glass for observation in the tests, and the bottom of the flume is made of impermeable concrete. An Acoustic Doppler Velocimeter (ADV, Fig. 5) was used to monitor the depth averaged flow velocity in the flume. The ADV was deployed 3 m upstream to the GMFP model in the symmetry plane of the flume. The sampling point of the ADV was 0.16 m above the bottom of the flume. The full range of the ADV was ±1 m/s. The accuracy of the ADV is ±0.5% of the measured value ± 1 mm/s and the sampling rate was 100 Hz. Some particles were added to the flume before the test to provide sufficient reflective particles for the ADV and thus to improve the data quality. The size of the particles was 0.1 mm and the density was 1.05×10^3 kg/m^3.

The GMFP model was deployed 20 m downstream to the entrance of the flume (Fig. 4). The GMFP model consisted of a model mattress, a model floating plate, and a series of strings connecting them. The width of the GMFP model was 0.8 m, which was identical to that of the flume. The model mattress was 0.26 m long and was composed of 10 mattress tubes filled with fine sand. The mattress tubes were sealed on both ends. Four model floating plates with different heights were used in the experiments. The height of the plates (H_p) were 0.08 m, 0.10 m, 0.12 m, and 0.16 m. The model plates were made of fiberglass and were regarded as rigid bodies in the tests. In this study, the sloping angle of the plate and the height of the sand-pass opening were adjusted manually by fixing the model plate.

In this study, the near bottom velocity on the leeside of the GMFP was measured to reveal the parametric effects of the GMFP on the flow pattern downstream to the device. As the ADV may underestimate the flow velocity in near-bottom regions (Precht et al., 2006), a LGY-II propeller-type current meter (Nanjing Hydraulic Research Institute, Nanjing, China) was used to measure the near bottom velocity on the leeside of the GMFP. The propeller diameter of the current meter is 1.5 cm. The full range of the current meter is 2.0 m/s, and the accuracy is ±1.5%. The starting velocity of the propeller is 0.01 m/s. The sampling time was 60 s. For each testing point, the near bottom velocity was measured twice to reduce the random error. If the difference between

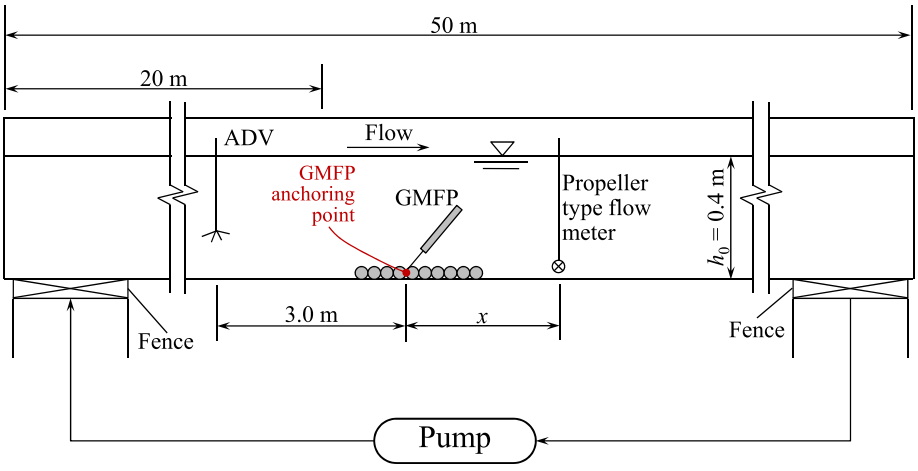

(a) Test flume

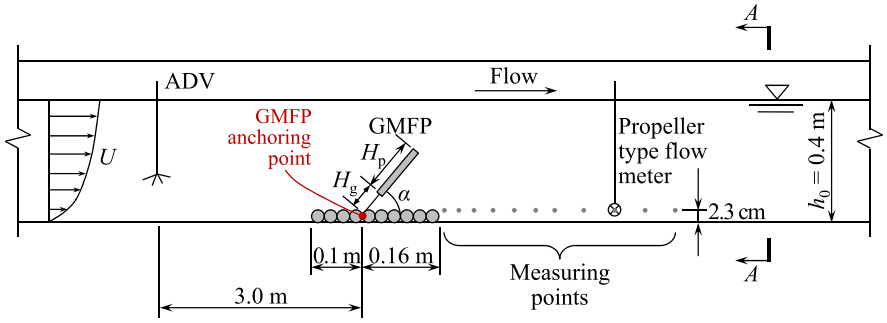

(b) Experimental setup

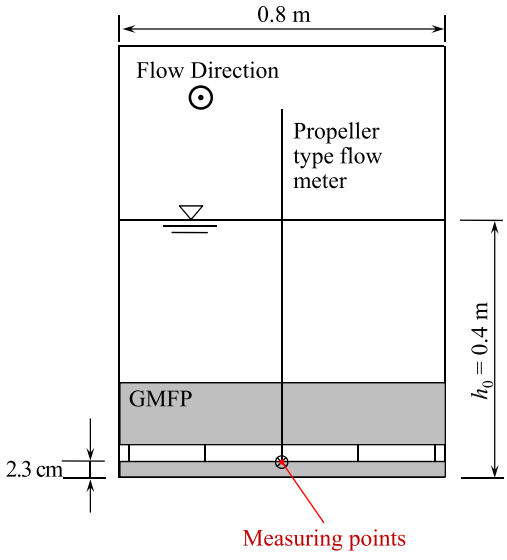

(c) Cross section *A*-*A* of the flume

Fig. 4. Sketch of the experiment setup (not to scale).

the two results was over 10%, the test case was repeated for a third time.

The horizontal distance between the testing points and the anchoring point of the GMFP was between 16 cm and 155 cm. In cases with large plate height (H_p = 0.12 m and 0.16 m), more testing points were measured, and the testing points extended up to 205 cm downstream to the GMFP. Thus, the testing points covered a range of bed from the downstream edge of the mattress to at least 10 times the plate height downstream to the GMFP. The range of the testing points was selected based on previous test and simulation results (Xie and Liu, 2010; Xie et al., 2019b). The testing points were located in the symmetry plane of the flume. The vertical location of all the testing points was 2.3 cm from the bottom of the flume, which is at the same height as the top surface of

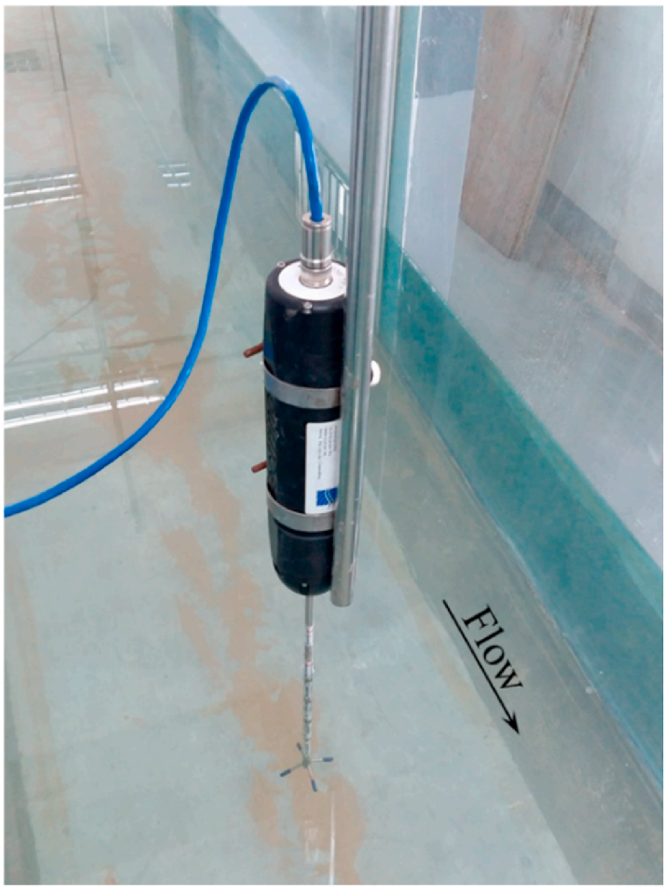

Fig. 5. (Color) Acoustic Doppler Velocimeter (ADV) used in the experiment. (For interpretation of the references to colour in this figure legend, the reader is referred to the Web version of this article.)

the mattress (Fig. 4).

2.2. Dimensional analysis

According to the protection mechanism of the floating flow-deflection devices similar to the GMFP, the bottom vortex is the dominant effect on the flow field downstream to the structure (Wang et al., 2015; Xie et al., 2019b). The reattachment point of the bottom vortex (Fig. 3) is the downstream end of the vortex, and generally reflects the dimension of the vortex. Thus, the location of the bottom vortex reattachment point was thus selected as the key parameter to describe the flow characteristics near the GMFP. In this study, the location of the reattachment point was described by the distance between the anchoring point of the GMFP and the reattachment point of the bottom vortex, denoted by x_0 (Fig. 3). Similar definitions were also adopted by previous studies on other floating flow deflecting structures (Li and Yu, 2009; Wang et al., 2015).

A dimensional analysis was carried out to identify the most important effects on the location of the reattachment point. Four dimensionless parameters were identified in this study based on the rule of dimensional homogeneity, and their effects on the location of the reattachment point x_0 were examined:

$$\frac{x_0}{H_p} = f\left(\alpha, \frac{H_p}{h_0}, \delta, Fr\right) \tag{1}$$

where H_p = the height of the floating plate (Fig. 4); α = the sloping angle; h_0 = the flow depth, and $h_0 = 0.4$ m for all cases in this study; H_p/h_0 = the relative plate height; δ = the opening ratio, defined as

$$\delta = \frac{H_g}{H_p + H_g} \tag{2}$$

where H_g = the height of the sand-pass gap between the floating plate and the mattress (Fig. 4); Fr = the Froude number, calculated by

$$Fr = \frac{U}{\sqrt{gh_0}} \tag{3}$$

where U = the depth averaged approaching flow velocity; g = gravitational acceleration, and $g = 9.8$ m/s^2.

In addition to the parameters mentioned above, some other parameters were also identified in the dimensional analysis, including the configurations of the geotextile mattress, the flow depth, and the roughness of the flume bed. However, these parameters were kept constant in all test cases in this study, or have been proved to have limited effect on the flow pattern downstream to the structure, so they were not discussed in this study.

In this study, the flow pattern near the GMFP in an open channel was modeled, and the Froude's law was thus used to determine the scale ratio. The length scale was determined to be model:prototype = 1:10, and the velocity scale was model:prototype = 1:3.16. All the parameters examined in this study complied with this scaling ratio. The effects of scaling on the accuracy of the test results were acceptable for this study.

2.3. Experimental cases

To investigate the effects of the GMFP design parameters on the flow pattern on the leeside of the GMFP, a total of 36 test cases were designed for the experiment (Table 1). The GMFP design parameters include the sloping angle of the plate (α), the relative plate height (H_p/h_0), and the opening ratio (δ). The definition of these parameters can be found in Section 2.2. In this study, the flow depth was $h_0 = 0.4$ m for all test cases, and three different flow velocity values were used. The depth-averaged flow velocity U varied between 0.3 m/s and 0.4 m/s for different cases. The Froude number for the test cases was between 0.152 and 0.202. Before the GMFP model was deployed in the flume, the undisturbed near bottom velocity u_0 in the three flow conditions was measured respectively. The undisturbed near bottom velocity was measured with the

Table 1
Experiment cases.

Group	Sloping angle α (°)	Relative plate height H_p/h_0	Opening ratio δ	Froude number Fr
A	35	0.25	0.231	0.152, 0.177, 0.202
	40	0.25	0.231	0.202
	45	0.25	0.231	0.152, 0.177, 0.202
	50	0.25	0.231	0.152, 0.177, 0.202
	55	0.25	0.231	0.202
	60	0.25	0.231	0.152, 0.177, 0.202
B	50	0.20	0.231	0.152, 0.177, 0.202
	50	0.25	0.231	0.152, 0.177, 0.202
	50	0.30	0.231	0.152, 0.177, 0.202
	50	0.40	0.231	0.152, 0.177
C	50	0.25	0.167	0.152, 0.177, 0.202
	50	0.25	0.231	0.152, 0.177, 0.202
	50	0.25	0.286	0.152, 0.177, 0.202
	50	0.25	0.333	0.152, 0.202

propeller type current meter in the same way as was measured downstream to the GMFP in the test cases. The measuring point was 2.3 cm above the bottom of the flume. The test cases were divided into three groups. In each group, only one GMFP design parameter was changed, and the other GMFP parameters were kept constant. Group A focused on the sloping angle of the GMFP, where the sloping angle α varied between 35° and 60°; Group B the height of the floating plate, where the relative plate height H_p/h_0 was between 0.20 and 0.40; Group C the opening ratio, where the opening ratio δ ranged between 0.167 and 0.333. The selection of the test parameters was based on previous studies on the GMFP (Xie et al., 2019a; Zhu et al., 2020). Further details of the test cases can be found in Table 1.

3. Test results

3.1. Effects of the sloping angle on the flow pattern downstream to the GMFP

The test cases in Group A were designed to investigate the effect of the sloping angle on the flow pattern on the leeside of the GMFP. The sloping angle of the GMFP α varied between 35° and 60°, and the other two design parameters of the GMFP were kept constant: the opening ratio $\delta = 0.231$ and the relative plate height $H_p/h_0 = 0.25$. Three different flow conditions were adopted in the test cases, in which the Froude number was 0.152, 0.177 and 0.202.

Fig. 6 shows the near bottom velocity distribution on the leeside of the GMFP for different sloping angles of the floating plate. The horizontal axis indicates the normalized distance to the anchoring point of the GMFP x/H_p (Fig. 4), and the vertical axis is the normalized near bottom velocity u/u_0, where u_0 is the undisturbed near bottom velocity. The test results show that the flow pattern on the leeside of the GMFP for different sloping angle values is similar. The near bottom velocity is close to zero near the downstream edge of the geotextile mattress. Immediately downstream to the mattress, there is an area in which the near bottom flow heads upstream. This area is the coverage of the bottom vortex. The near bottom flow turns to the downstream side on the leeside of the bottom vortex and enters the low velocity zone. The near bottom velocity steadily climbs up as the measuring points moves further downstream in the low velocity zone (Fig. 6). However, the near bottom velocity is still at least 25% lower than the undisturbed near bottom velocity at 15–20 times the plate height downstream to the GMFP in different configurations, which agrees well with the simulation results of Xie and Liu (2010). The area affected by the GMFP actually covers at least 20 times the plate height downstream.

The length of the bottom vortex is observed to vary remarkably with the sloping angle and the Froude number. When the sloping angle rises from 35° to 45°, the bottom vortex extends downstream gradually. The downstream edge of the bottom vortex moves to the leeside, but the variation of the upstream end of the bottom vortex is not remarkable. When the sloping angle is over 45°, the extension of the bottom vortex slows down with further increase of the sloping angle. The extension of the bottom vortex is also observed when the Froude number increases and the other parameters are fixed. Similar variations of the vortex magnitude can also be seen in those near bridge piers due to the changes of flow parameters and pier properties (Tafarojnoruz et al., 2012; Tafarojnoruz and Gaudio, 2012; Tafarojnoruz and Agostino, 2020). The variation of the sloping angle affects the maximum reversed velocity near the bed as well. The maximum reversed velocity shows an increasing trend with an increasing sloping angle, which may indicate a more intensified bottom vortex. The increasing sloping angle also generally slows down the near bottom flow in the low velocity zone.

The reattachment point of the bottom vortex is the downstream edge of the bottom vortex (Fig. 3), where the near bottom flow reverses and begins to head downstream. Fig. 7 shows the movement of the reattachment point with the sloping angle in different flow conditions. The reattachment point was obtained by the linear interpolation of the near bottom velocity curve in Fig. 7. Herein, the horizontal axis indicates the sine value of the sloping angle, which reflects the blockage area of the sloping plate for fixed plate dimensions. The vertical axis is the normalized horizontal distance between the reattachment point and the anchoring point of the GMFP (x_0/H_p). The location variation of the reattachment point varies in a similar pattern in three flow conditions. The reattachment point moves downstream when the Froude number increases from 0.152 to 0.177, but the effect of the Froude number was not obvious when the Froude number further increases from 0.177 to 0.202. When the sloping angle increases from 35° ($\sin\alpha = 0.57$) to 50° ($\sin\alpha = 0.77$), the reattachment point moves to the downstream side. Then the reattachment moves upstream slightly with further increase of

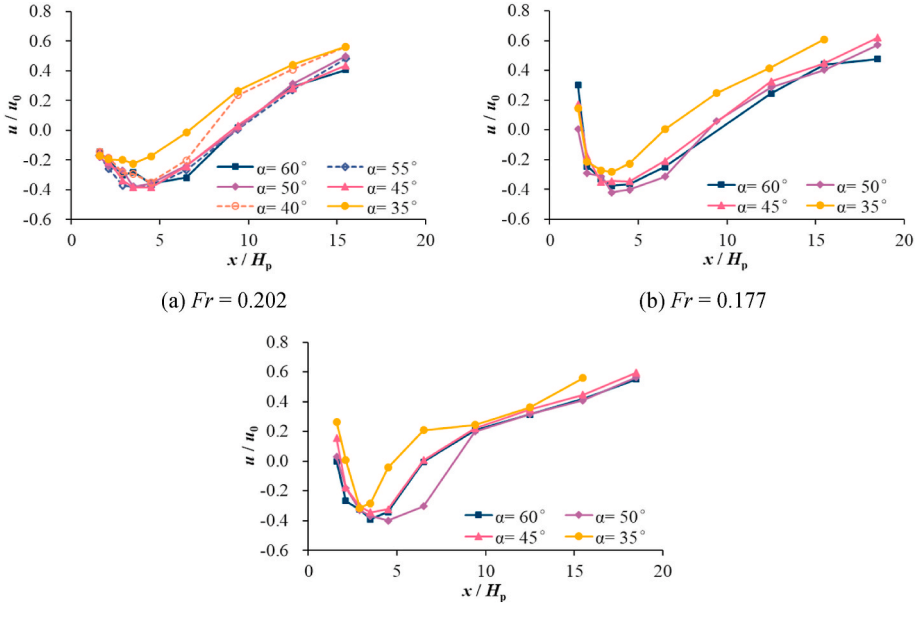

(a) $Fr = 0.202$ (b) $Fr = 0.177$

(c) $Fr = 0.152$

Fig. 6. Near bottom velocity distribution for different sloping angle.

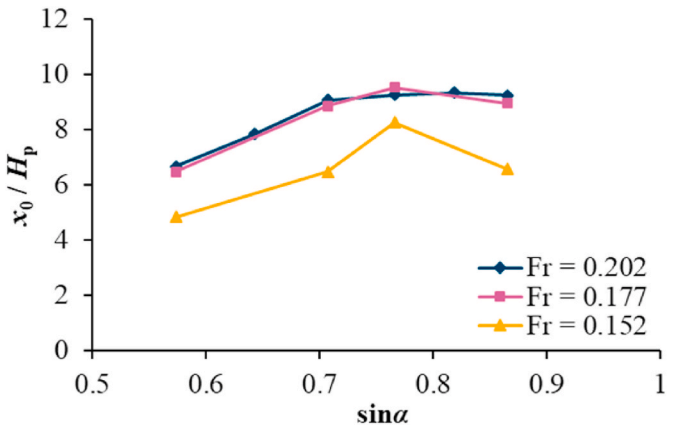

Fig. 7. Relationship between the reattachment point location and the sloping angle.

the sloping angle. All three curves hit a zenith near $\sin\alpha = 0.77$ ($\alpha = 50°$), where the coverage of the bottom vortex reaches maximum within the range of test parameters in this test group. This phenomenon may be attributed to the variation of the bottom vortex with the increase in the blockage of the floating plate, and is discussed in Section 4.1.

3.2. Effects of the plate height

The test cases in Group B were designed to investigate the effect of the plate height on the flow pattern on the leeside of the GMFP. The height of the floating plate H_p varied between 8 cm and 16 cm, and the relative plate height H_p/h_0 was between 0.2 and 0.4, where $h_0 = 0.4$ m is the flow depth. The other two design parameters of the GMFP were kept constant: the sloping angle $\alpha = 50°$ and the opening ratio $\delta = 0.231$. Three different flow conditions were adopted in the test cases, in which the Froude number was 0.152, 0.177 and 0.202.

Fig. 8 shows the near bottom velocity distribution on the leeside of the GMFP for different heights of the floating plate. The test results imply that the flow pattern on the leeside of the GMFP for different plate heights is basically similar to those in Fig. 6. A remarkable decrease in the coverage of the bottom vortex can be observed with a rising plate height when the relative plate height $H_p/h_0 \geq 0.25$. Compared with the results in Fig. 6, the variation in the upstream edge of the bottom vortex is more significant when the plate height is changed. In some cases, high velocity near bottom flow was detected near the downstream edge of the mattress, which is discussed in Section 4.2.

Excepting the cases in which the velocity near the mattress was high, the maximum reversed velocity in the bottom vortex climbs with the increase of the plate height. The coverage of the bottom vortex shows a positive correlation with the Froude number. The effects of the Froude number and the plate height on the velocity in the low velocity zone is not obvious.

Fig. 9 shows the movement of the reattachment point with the relative plate height in different flow conditions. The horizontal axis indicates the relative plate height H_p/h_0. The movement pattern of the reattachment point is almost identical in different flow conditions. The results show that the reattachment point moves downstream when the relative plate height increases from $H_p/h_0 = 0.20$ to $H_p/h_0 = 0.25$. After that, the reattachment point retreats considerably upstream when the

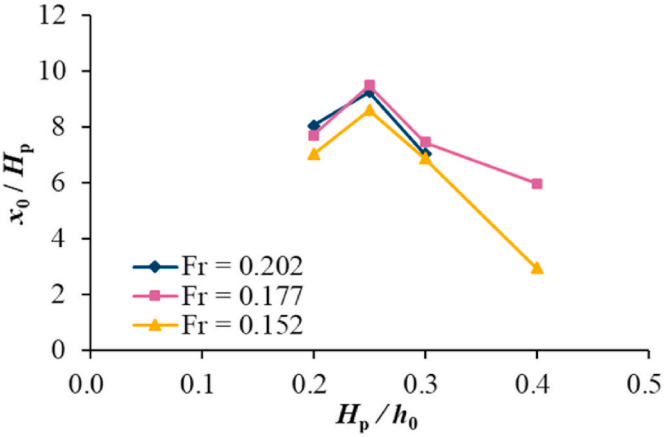

Fig. 9. Relationship between the reattachment point location and the plate height.

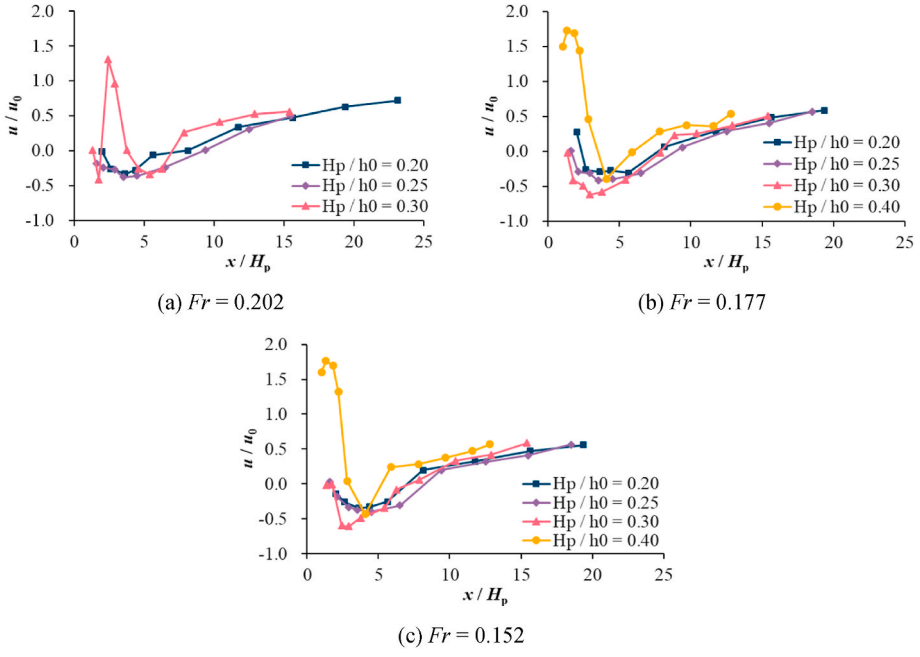

(a) $Fr = 0.202$ (b) $Fr = 0.177$

(c) $Fr = 0.152$

Fig. 8. Near bottom velocity distribution for different plate height.

relative plate height further increases to $H_p/h_0 = 0.40$. The retreat of the reattachment point x_0/H_p with the increase of the relative plate height H_p/h_0 can partially be attributed to the normalization of the reattachment point with the plate height. With the increase of the plate height H_p, x_0/H_p can decrease when the increase rate of x_0 is smaller than that of H_p. The retreat of the bottom vortex with larger obstruction height of the floating plate can also be observed in the results of Group A, but the retreat of bottom vortex with increasing plate height is more obvious. Further discussion on the relationship between the blockage of the floating plate and the location of the reattachment is proposed in Section 4.1.

3.3. Effects of the opening ratio

The test cases in Group C were designed to investigate the effect of the opening ratio on the flow pattern on the leeside of the GMFP. The opening ratio δ varied between 0.167 and 0.333. The other two design parameters of the GMFP were kept constant: the sloping angle $\alpha = 50^\circ$ and the relative plate height $H_p/h_0 = 0.25$. Three different flow conditions were adopted in the test cases, in which the Froude number was 0.152, 0.177 and 0.202.

Fig. 10 shows the near bottom velocity distribution on the leeside of the GMFP for different opening ratio. The variation pattern of the reattachment location is almost identical in different flow conditions. In general, the coverage of the bottom vortex gradually retreats with an increasing opening ratio. When the opening ratio increases from 0.167 to 0.231, the variation in the coverage of the bottom vortex was not obvious. However, the variation of the bottom vortex coverage becomes remarkable when the opening ratio climbs over $\delta = 0.231$. This phenomenon coincides with the test results of Zhu et al. (2020). The maximum reversed velocity of the bottom vortex also shows a negative correlation with the opening ratio when $\delta \geq 0.231$. In addition, the flow velocity on the leeside of the bottom vortex increases with the increasing opening ratio. The coverage of the bottom vortex shows a positive correlation with the Froude number.

Fig. 11 shows the movement of the reattachment point with the opening ratio in different flow conditions. The variation pattern of the reattachment location is almost identical in different flow conditions. The results show that when the opening ratio δ increases from $\delta = 0.167$ to $\delta = 0.231$, the movement of the reattachment point is not obvious. The reattachment point moves upstream considerably when the opening ratio δ increases over 0.231. The variation pattern of the reattachment point agrees with the results of Zhu et al. (2020). Zhu et al. (2020) found that the flow through the sand-pass gap gradually intensifies when the opening ratio increases from $\delta = 0.231$. The intensity of the bottom vortex gradually descends due to the disturbance of the intensified bottom flow. In this study, the maximum reversed bottom velocity and the coverage of the bottom vortex show a negative correlation with the opening ratio for $\delta \geq 0.231$, which is consistent with the conclusion drawn by Zhu et al. (2020).

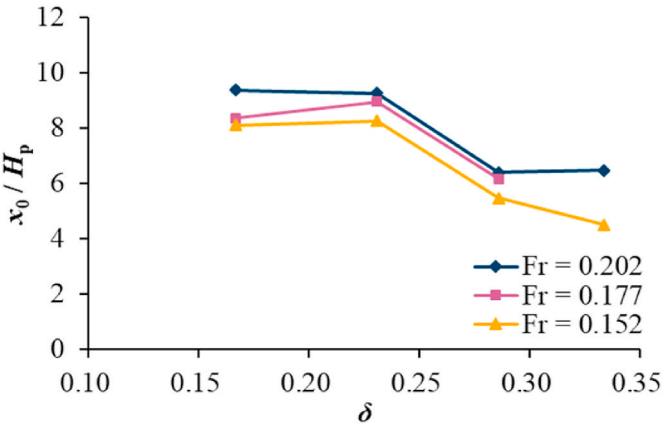

Fig. 11. Relationship between the reattachment point location and the opening ratio.

4. Discussion

4.1. Effects of the plate obstruction height on the reattachment point

The relationship between the length of the bottom vortex and the obstruction height of other flow deflection devices has been discussed in previous studies (Li and Yu, 2009; Wang et al., 2015). However, the previous results cannot necessarily be directly applied to the GMFP due

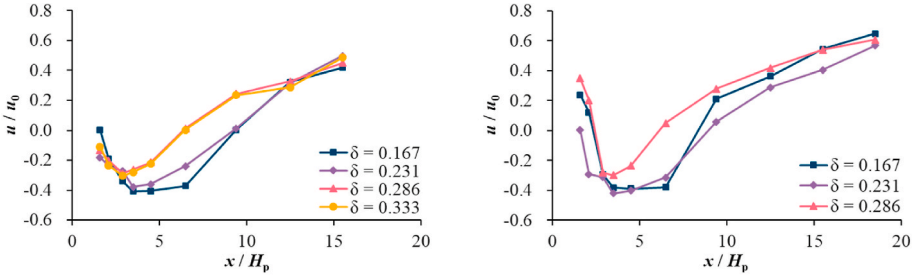

(a) $Fr = 0.202$ (b) $Fr = 0.177$

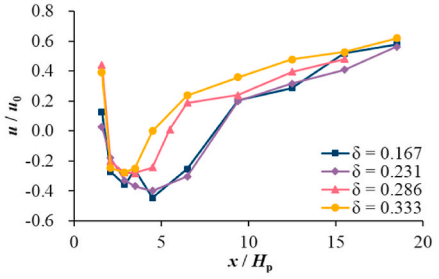

(c) $Fr = 0.152$

Fig. 10. Near bottom velocity distribution for different opening ratio.

to the differences in the flow pattern between the GMFP and the previously studied structure. In addition, the sloping angle of the floating plate is treated as an independent variable in this study, which can bring distinctions to the variation pattern of the bottom vortex dimension with the obstruction height. Thus, the effect of the GMFP obstruction height is analyzed below based on the results in Figs. 6 and 8.

Fig. 12 shows the variation of the reattachment point location x_0/H_p with the relative obstruction height $H_p\sin\alpha/h_0$. The results in Figs. 6 and 8 are included. The obstruction height is normalized in the same way as that in previous studies (Xie et al., 2019b; Zhu et al., 2020). Fig. 12 indicates that variation pattern of the reattachment with the obstruction height is similar for the different Froude numbers tested in this study. The location of the reattachment point tends to move downstream with the increase of the obstruction height when $H_p\sin\alpha/h_0$ is below 0.2, and then retreats to the upstream side. The downstream limit of the reattachment point is reached when the relative obstruction height $H_p\sin\alpha/h_0$ is near 0.2. With the increase of the Froude number, the reattachment point moves to the downstream side steadily. In Fig. 12, the test results in different flow conditions are close to each other, which indicates that the effects of the Froude number on the reattachment point may be not as remarkable as that of the obstruction height.

When the obstruction height of the floating plate is below 0.2, the bottom vortex extends with increasing obstruction height, which can mainly be attributed to the separation of flow passing objects with sharp corners at the section corners. With the increase of the obstruction height, the separation point of the flow over the floating plate rises, and the bottom vortex extends to the leeside. When the obstruction height is over 0.2, the retreat of the reattachment point with the obstruction height may be associated with two factors. The first potential factor is the variation of the water surface profile (Fig. 13). With the increase the obstruction height, the blockage effect of the floating plate on the water surface profile becomes increasingly significant. Drawdown occurs at the GMFP. The water surface rises up on the upstream side of the GMFP and drops on the downstream side, which was observed in previous investigations on the GMFP (Xie et al., 2019a). As the blockage effect continues intensifying, the water surface profile over the GMFP gets steeper. A similar phenomenon was observed over a submerged horizontal cylinder in steady current (Chiew, 1991; Zhu and Xie, 2015). Consequently, the streamline at the separation point on the top of the floating plate can also incline more steeply towards bed. As the bottom vortex is partially dominated by the flow pattern on the top of the floating plate, the bottom vortex can thus retreat and the reattachment point can move upstream. The other potential factor is the intensified flow through the sand-pass gap between the mattress and the floating plate. The strengthened blockage effect due to the increasing obstruction height may accelerate the bottom flow through the sand-pass gap, which may cause the descent of the bottom vortex intensity (Zhu et al., 2020),

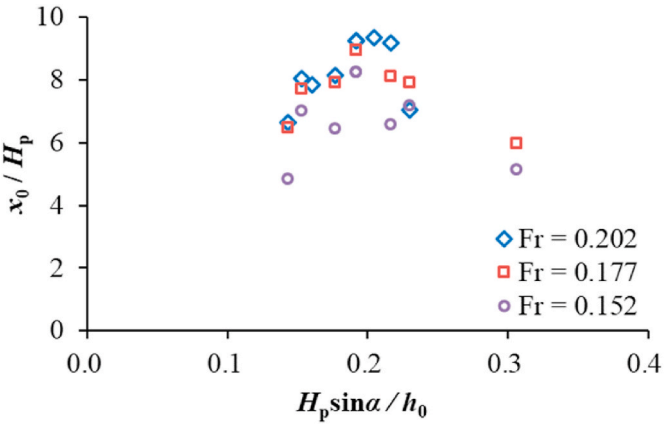

Fig. 12. Relationship between the plate obstruction height and the location of the reattachment point.

and thus the retreat of the reattachment point.

Based on the relationship analyzed in Fig. 12, an empirical equation is proposed for the location of the reattachment point and the obstruction height of the floating plates:

$$x_0 / H_p = \left[-497\left(H_p \sin\alpha / h_0\right)^2 + 205\left(H_p \sin\alpha / h_0\right)\right] Fr^{0.575} \quad (4)$$

Fig. 14 shows the comparison between the measured location of the reattachment point and the predicted results by Eq. (4). The results show that the prediction of Eq. (4) is reasonable and all the data points fall within the 20% deviation lines. The application range of Eq. (4) is $0.15 \le H_p\sin\alpha/h_0 \le 0.30$. It should be noted that the data points in Fig. 12 do not fall on a single curve, which indicates that the location of the reattachment point is also affected by other parameters except for the obstruction height of the GMFP and the Froude number. Further studies are needed to reveal more details in the variation mechanism of the reattachment point location.

4.2. Effects of the plate height on the high velocity flow near the mattress

The results of test group B detect high velocity bottom flow near the downstream edge of the geotextile mattress in test cases with large plate height (H_p/h_0 = 0.30 and 0.40). The maximum near bottom velocity near the edge of the mattress reaches over 1.5 times the undisturbed velocity (Fig. 8(b and c)). This phenomenon can be explained as follows:

With the increase of the plate height, the blockage effect of the floating plate becomes increasingly more remarkable. The increased plate height narrows the passage of the approaching flow, while the total flow rate in the flume remains unchanged. The flow over the floating plate and through the sand-pass gap is thus accelerated. In addition, the GMFP is deployed in an open channel flow in this study, where the flow depth is limited. The blockage effect is further enhanced due to the limited space between the water surface and the floating plate. Thus, the flow velocity through the sand-pass gap and over the floating plate significantly increases. When the geotextile mattress is not long enough to cover the area affected by the high velocity gap flow (Xie et al., 2013), high velocity bottom flow near the edge mattress appears.

The results in Fig. 8 may also imply the existence of a critical plate height for the appearance of the local high velocity flow. The high velocity near bottom flow appears when the plate height is over this critical value. In Fig. 8(b and c), when the averaged flow velocity in the flume is 0.30 m/s (Fr = 0.152) and 0.35 m/s (Fr = 0.177), the high velocity near the edge of the mattress appears when H_p = 16 cm, but does not appear when H_p = 12 cm. When the averaged flow velocity in the flume increases to 0.40 m/s (Fr = 0.202), the high velocity appears when H_p = 12 cm. This comparison indicates that the high velocity flow is more likely to appear for higher approaching flow velocity when the plate height is fixed. In other words, the increase of the flow rate through the flume can lead to a decrease in the critical plate height. As the high velocity flow is also reported to be closely associated with the opening ratio (Xie et al., 2013; Zhu et al., 2020), the critical plate height is a function of both the opening ratio and the Froude number.

High velocity near the edge of the mattress may bring considerable negative effects to the safety of the GMFP and the structure protected. Local scour can appear near the mattress. The GMFP can thus be more vulnerable to the seepage failure underneath the mattress (Xie et al., 2019a), which can destabilize the GMFP structure. In the cases where high velocity appears, the protection effects of the GMFP are influenced. The dimension of the bottom vortex decreases. The upstream edge of the bottom vortex retreats to the leeside. Thus, the obstruction height should be selected within a reasonable range to prevent the high velocity flow near the edge of the mattress. For the conditions tested in this research, the ideal relative obstruction height is about 0.20.

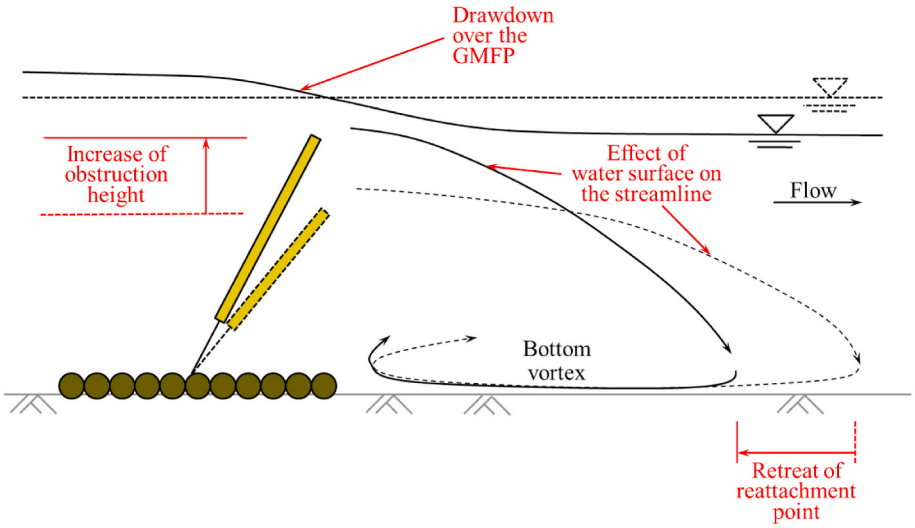

Fig. 13. Effect of the water surface on the retreat of the reattachment point.

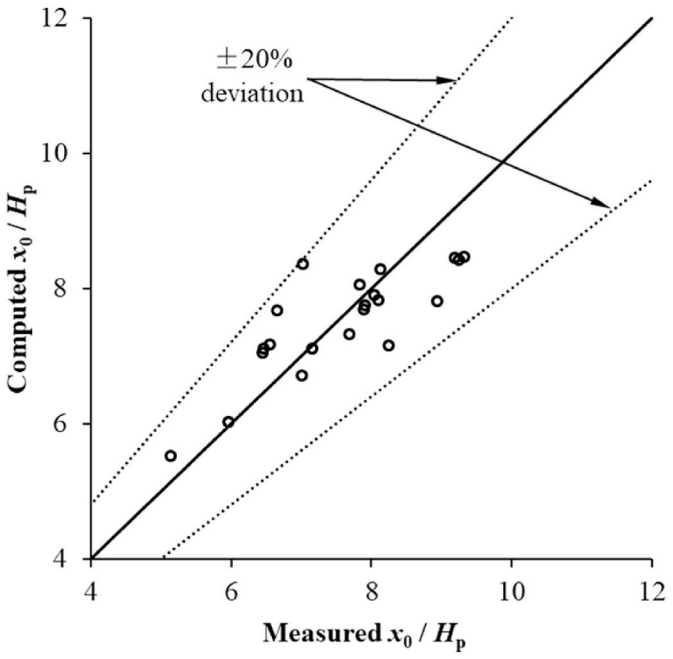

Fig. 14. Comparison between the measured location of the reattachment point and the predicted values.

5. Conclusion

The parametric effects on the flow pattern downstream to the GMFP was investigated with the near bottom velocity close to the structure. The effects of the GMFP design parameters were investigated, including the sloping angle, the height of the floating plate, and the opening ratio. The following conclusions can be achieved based on the results and discussion above:

1. The bottom vortex generated by the GMFP is detected immediately downstream to the mattress in most cases. The near bottom velocity in the low velocity zone downstream to the bottom vortex is at least 25% lower than the undisturbed near bottom velocity. The effects of the GMFP extend to at least 20 times the plate height downstream.
2. The reattachment point of the bottom vortex moves downstream when the sloping angle increases from 35° ($\sin\alpha = 0.57$) to 50° ($\sin\alpha = 0.77$), and reaches a downstream limit near $\sin\alpha = 0.77$ ($\alpha = 50°$) in the tested range of parameter of this study.
3. The reattachment point moves downstream when the plate height increases from $H_p/h_0 = 0.20$ to $H_p/h_0 = 0.25$, and steadily retreats with the further increase of the plate height.
4. Within the range of hydrodynamic parameters tested in this study, the reattachment point moves upstream considerably when the opening ratio δ increases over 0.231, which agrees with the conclusion of previous studies.
5. The reattachment point tends to move downstream with the increase of the obstruction height of the floating plate, and then retreats to the upstream side. The downstream limit of the reattachment point is reached when the relative obstruction height is about $H_p\sin\alpha/h_0 = 0.2$. The variation pattern may be attributed to the variation in the water surface profile and the enhanced flow through the sand-pass gap. An equation was proposed to predict the relationship between the obstruction height and the reattachment location. The critical relative obstruction height for the downstream limit of the reattachment point ($H_p\sin\alpha/h_0 = 0.2$) need to be evaluated with more test data in further investigations.
6. A branch of high velocity flow was observed near the downstream edge of the geotextile mattress in the test cases with large plate height, which may be attributed to the enhanced flow through the sand-pass gap due to the intensified blockage effect. The ideal relative plate height for the parameter tested in this study is about 0.2.

CRediT authorship contribution statement

Yehui Zhu: Conceptualization, Methodology, Validation, Formal analysis, Investigation, Resources, Data curation, Writing – original draft, Writing – review & editing, Visualization, Funding acquisition. **Liquan Xie:** Conceptualization, Methodology, Validation, Formal analysis, Investigation, Resources, Writing – review & editing, Supervision, Funding acquisition. **Tsung-chow Su:** Resources, Writing – review & editing.

Declaration of competing interest

The authors declare that they have no known competing financial interests or personal relationships that could have appeared to influence the work reported in this paper.

Data availability

Data will be made available on request.

Acknowledgements

Funding: This work was supported by the National Natural Science Foundation of China [grant numbers 11172213 and 51479137], the China Scholarship Council [grant number 201806260166].

The funders had no role in study design, data collection and analysis, decision to publish, or preparation of the manuscript.

References

Biswas, P., Barbhuiya, A.K., 2018. Countermeasure of river bend scour using a combination of submerged vanes and riprap. Int. J. Sediment Res. 33, 478–492. https://doi.org/10.1016/j.ijsrc.2018.04.002.

Cai, Y., Cao, Z., Wang, Y., Guo, Z., Chen, R., 2018. Experimental and numerical study of the tidal bore impact on a newly-developed sheet-pile groin in Qiantang river. Appl. Ocean Res. 81, 106–115. https://doi.org/10.1016/j.apor.2018.10.003.

Chiew, Y.M., 1991. Flow Around Horizontal Circular Cylinder in Shallow Flows. Journal of Waterway, Port, Coastal, and Ocean Engineering 117 (2), 120–135. https://doi.org/10.1061/(ASCE)0733-950X(1991)117:2(120).

Galan, A., Simarro, G., Sanchez-Serrano, G., 2015. Nonburied riprap mattress sizing for single piers in the presence of bedforms. J. Hydraul. Eng. 141, 06015004 https://doi.org/10.1061/(ASCE)HY.1943-7900.0001003.

Jafarnejad, M., Franca, M., Pfister, M., Schleiss, A., 2019. Design of riverbank riprap using large, individually placed blocks. J. Hydraul. Eng. 145, 04019042 https://doi.org/10.1061/(ASCE)HY.1943-7900.0001641.

Khajenoori, L., Wright, G., Crapper, M., 2021. Laboratory investigation of geobag revetment performance in rivers. Geosciences 11, 304. https://doi.org/10.3390/geosciences11080304.

Kiss, T., Amissah, G., Fiala, K., 2019. Bank processes and revetment erosion of a large lowland river: case study of the lower Tisza River, Hungary. Water 11, 1313. https://doi.org/10.3390/w11061313.

Lee, W.L., Lu, C.W., Huang, C.K., 2021. A study on interaction between overfall types and scour at bridge piers with a moving-bed experiment. Water 13, 152. https://doi.org/10.3390/w13020152.

Li, C., Shih, R.S., Weng, W.K., Liao, T.W., 2021. Analysis of vortex formation and energy dissipation during interaction of solitary-like waves with submerged breakwaters based on particle image velocimetry. Appl. Ocean Res. 110, 102579. https://10.1016/j.apor.2021.102579.

Li, Y., Yu, G., 2009. Experimental investigation on flow characteristics at leeside of suspended flexible curtain for sedimentation enhancement. China Ocean Eng. 23, 565–576.

Ma, A., Cao, M., Deng, Y., Xu, Y., Yang, S., Hu, Y., Chang, L., 2021. Laboratory and field investigation of an ecological cavity mattress in river bed protection. Ecol. Eng. 172, 106393 https://doi.org/10.1016/j.ecoleng.2021.106393.

Precht, E., Janssen, F., Huettel, M., 2006. Near-bottom performance of the Acoustic Doppler Velocimeter (ADV) – a comparative study. Aquat. Ecol. 40, 481–492. https://doi.org/10.1007/s10452-004-8059-y.

Rashno, E., Zarrati, A., Tabarestani, M., 2020. Design of riprap for bridge pier groups. Can. J. Civ. Eng. 47, 516–522. https://doi.org/10.1139/cjce-2019-0007.

Tafarojnoruz, A., Agostino, L., 2020. Large eddy simulation of the turbulent flow field around a submerged pile within a scour hole under current condition. Coast Eng. J. 62, 489–503. https://doi.org/10.1080/21664250.2020.1807453.

Tafarojnoruz, A., Gaudio, R., 2012. Discussion on "Vortex scouring process around bridge pier with a caisson". J. Hydraul. Res. 50, 443–444. https://doi.org/10.1080/00221686.2012.707795.

Tafarojnoruz, A., Gaudio, R., Calomino, F., 2012. Effects of a slotted bridge pier on the approach flow, in: XXXIII Convegno Nazionale di Idraulica e Costruzioni Idrauliche IDRA 2012. Brescia 1–10, 10–14 September, 2012.

Wang, H., Si, F., Lou, G., Yang, W., Yu, G., 2015. Hydrodynamic characteristics of a suspended curtain for sediment trapping. J. Waterw. Port, Coast. Ocean Eng. 141, 04014030 https://doi.org/10.1061/(ASCE)WW.1943-5460.0000270.

Wu, T., Sun, H., Cai, Y., Wu, J., Zhang, Y., 2022. Analytical study on the dynamic responses of a sheet-pile groin subjected to transient lateral impulses. Ocean Eng. 249, 110875 https://doi.org/10.1016/j.oceaneng.2022.110875.

Xie, L., Huang, W., Yu, Y., 2013. Experimental study of sediment trapping by geotextile mattress installed with sloping curtain. Geosynth. Int. 20, 389–395. https://doi.org/10.1680/gein.13.00026.

Xie, L., Liu, S., 2010. Stability of sand beds around mattress-curtain sets. In: OMAE2010. 29th Int. Conf. Ocean, Offshore and Arctic Eng., 1, pp. 839–844. https://doi.org/10.1115/OMAE2010-20872.

Xie, L., Zhu, Y., Huang, W., Liu, C., 2015. Experimental investigations of dynamic wave force on seabed around a geotextile mattress with floating curtain. J. Coast Res. 73, 35–39. https://doi.org/10.2112/SI73-007.1.

Xie, L., Zhu, Y., Li, Y., Su, T.C., 2019a. Experimental study on bed pressure around geotextile mattress with sloping plate. PLoS One 14, e0211312. https://doi.org/10.1371/journal.pone.0211312.

Xie, L., Zhu, Y., Su, T.C., 2019b. Scour protection of partially embedded pipelines using sloping curtains. J. Hydraul. Eng. 145, 04019001 https://doi.org/10.1061/(ASCE)HY.1943-7900.0001571.

Xue, S., Xu, Y., Xu, G., Wang, J., Chen, Q., 2022. A novel tri-semicircle shaped submerged breakwater for mitigating wave loads on coastal bridges part I: Efficacy. Ocean Eng. 245, 110462 https://doi.org/10.1016/j.oceaneng.2021.110462.

Zhang, R., Stive, M.J.F., 2019. Numerical modelling of hydrodynamics of permeable pile groins using SWASH. Coast. Eng. 153, 103558 https://doi.org/10.1016/j.coastaleng.2019.103558.

Zhao, E., Dong, Y., Tang, Y., Xia, X., 2021. Performance of submerged semi-circular breakwater under solitary wave in consideration of porous media. Ocean Eng. 223, 108573 https://doi.org/10.1016/j.oceaneng.2021.108573.

Zhu, Y., Xie, L., 2015. Numerical analysis of flow effects on water interface over a submarine pipeline. In: Xie, L. (Ed.), Resources, Environment and Engineering II: Proceedings of the 2nd Technical Congress on Resources, Environment and Engineering (CREE 2015). CRC Press, pp. 99–104.

Zhu, Y., Xie, L., Su, T.C., 2020. Scour protection effects of a geotextile mattress with floating plate on a pipeline. Sustainability 12, 3482. https://doi.org/10.3390/su12083482.